Journal of Radioanalytical and Nuclear Chemistry (2019) 319:997–1012
https://doi.org/10.1007/s10967-018-06403-7

Sorption behavior of some radionuclides using prepared adsorbent of hydroxyapatite from biomass waste material

D. M. Imam[1] · S. I. Moussa[1] · M. F. Attallah[1]

Received: 6 October 2018 / Published online: 2 January 2019

Abstract
We aim to recycle and utilization of eggshell as a biomass waste of human foodstuff. Pure hydroxyapatite nano-particles were prepared using waste eggshell at different temperature of 80 °C (ESHANP) and calcination at the 850 °C (CESHA) adsorbent materials and characterized by some instruments. Sorption studies of ^{60}Co and ^{109}Cd from aqueous waste solutions onto ESHANP and CESHA were performed at different pH solutions, initial ion concentration and contact time. The obtained data were analyzed using some kinetic, diffusion and isotherm models. It can be recommended ESHANP as remediation agent for nuclear waste sites.

Keywords Radioactive liquid waste · Removal · Utilization, biomass material, toxic heavy elements

Introduction

A numerous amounts of radionuclides were freed into the environment because of the operations of research reactors, accelerators, and laboratory activities. The resulting of high yield fission products may generate radioactive waste, is a significant radioactive contaminant at nuclear facilities worldwide [1, 2]. The released radionuclides are deposited on the soil, plant and water. Among them, long-lived radionuclides, such as ^{134}Cs ($t_{1/2}$: 2.06 year), ^{137}Cs ($t_{1/2}$: 30.17 year), and ^{90}Sr ($t_{1/2}$: 28.79 year), which are of bother in terms of environmental contamination. The disposal of this radioactive waste is among the most extreme costly environmental problems. There are diverse methods to remove metal ions from wastewater, natural ion exchange such as clay minerals; carbon materials, polymer materials, and oxides were extensively used [3] for radionuclides removal from nuclear/radioactive waste waters. However, these materials suffer from either low efficiencies or low adsorption capacities and inconsistent quality. Other technologies include precipitation ultrafiltration and osmosis [4] is often expensive.

Calcium apatite with a general chemical structure $Ca_{10-n}X_n(PO_4)_{6-m}Y_mZ_2$; X and Y represent cations (Sr(II), Na(I), Pb(II) and Cd(II) etc.) and anions (HPO_4^{2-} and CO_3^{2-} etc.) that can substitute for PO_4^{3-} groups in the main texture, while Z can be OH^-, F^-, C^-, or Br^- [5], have suitable properties for the immobilization of actinides & lanthanides radionuclides and poisonous metals, [6, 7]. As a result of strong adsorptive properties; big surface area, high stability, enhanced active sites, and abundant functional groups; it was increasingly used in the treatment of wastewater and nuclear waste [6, 8]. The surface of apatite could be used for sorbed or exchanged cationic radionuclides [9] and also anionic radionuclides [10, 11].

Metals (e.g., Pb, Sr, and Co) and actinides (e.g., U) can be sorbed onto the environmentally stable structure of hydroxyapatite nano-particles (HANP) [6, 8]. HANP has been assessed as a remediation agent for nuclear waste sites [8]. In addition, mobile HANP can alter the distribution of many metal contaminants in soils and groundwater [12]. Hydroxyapatite was shown to remove Sr(II) and Co(II) from water solution and artificial groundwater [8]. Sequestration of strontium-90 by hydroxyapatite was investigated with a mixture of calcium citrate & Na- phosphate by releasing Ca(II) ions [9]. Moderate sorption of As, Se, Sr, Cs and Tc, and very good removal of U and Pu by hydroxyapatite adsorbents were observed [13]. It can conclude that phosphate

Electronic supplementary material The online version of this article (https://doi.org/10.1007/s10967-018-06403-7) contains supplementary material, which is available to authorized users.

✉ M. F. Attallah
dr.m.f.attallah@gmail.com; mohamed.attallah@eaea.org.eg

[1] Hot Laboratories Center, Egyptian Atomic Energy Authority, Cairo 13759, Egypt

minerals especially hydroxyapatite are low-cost & friends of the environment amendments for immobilization of different radionuclides [14, 15]. There has been widespread interest in developing low cost alternatives from eggshell wastes [16, 17]. The recycling of hen eggshells not only reduced their waste, but also used for preparation nanomaterials. Another benefit is a route of improving the ecosphere [18]. The eggshells mainly enrich by calcium carbonate (91–94%), which makes it a suitable target as a Ca precursor such as CaO for synthesizing hydroxyapatite powder [19]. Therefore in this investigation, experimental procedures was made to synthesize pure hydroxyapatite nano-particles using waste eggshells as a Ca source.

The remediation of different radionuclides ^{60}Co and ^{109}Cd from radioactive waste using waste eggshell hydroxyapatite nano-particles is a key challenge for nuclear safeguards. It is essential to explore remediation strategies which show promise of removing or immobilizing most of problematic radionuclides.

The overall objective of this study was therefore focused on the synthesis of pure hydroxyapatite nano-particles using waste eggshell (ESHANP), fully characterize the properties of ESHANP using EDX, TG-DTA, SEM and FTIR. Application for the effective removal of ^{60}Co and ^{109}Cd from aqueous solutions; to investigate the efficiency of differently prepared hydroxyapatite for the sorptive of the ^{60}Co and ^{109}Cd radionuclides which are major contributors to radioactivity in nuclear wastes and contamination was studied. The effect of pH, shaking period and initial metal concentration on adsorption capacities of ^{60}Co and ^{109}Cd were also evaluated in batch adsorption modes to illustrate the performance of ESHANP to remove ^{60}Co and ^{109}Cd from aqueous solutions. A reaction mechanism for metals interaction with ESHANP was also proposed.

Materials and methods

Chemicals and reagents

All chemicals were A.G. (analytical grade) and were used without purification. The radioactive tracers of ^{60}Co(II) were provided by the Egyptian Second Nuclear Research Reactor. A weight of 1 mg ($CoCl_2$) was wrapped in a thin aluminum foil and irradiated using 10^{14} n cm^{-2} sec^{-1} neutron flux. After cooling, the irradiated sample was melted in DDW. ^{99}Mo and ^{99m}Tc radioisotopes have been supplied from the Radioisotopes Production Facility associated with 2nd Egyptian Nuclear Research Reactor at EAEA. The radioactivity of the prepared isotope was γ-counted using NaI scintillation counter connected to single channel spectrometer (Spectech ST 360 to crystal, USA).

Preparation of eggshells hydroxyapatite nanoparticles (ESHANP)

In this study, eggshells hydroxyapatite nanoparticle (ESHAP) was prepared by a neutralization method in the presences of ultrasonic irradiation. The experimental procedure is demonstrated as follows:

Preparation of CaO

Eggshells waste was pretreated with detergent, hexane and DDW after that, dried at 80.0 °C [20]. Appropriate amounts of it were calcinated at 1000 °C for 24 h, to eliminate organic matter. The eggshell evolves carbon dioxide beyond 850 °C and converted into calcium oxide [21], according to the following reaction:

$$\underset{\text{(eggshells)}}{CaCO_3} \rightarrow CaO + CO_{2_{(g)}} \quad (1)$$

Preparation of $Ca(OH)_2$

The white product (CaO) was finally grounded and the required quantity was allowed to mix with freshly DDW. The suspension $Ca(OH)_2$ was expected to form as shown by equation below:

$$CaO + H_2O \rightarrow Ca(OH)_2 + \text{heat} \quad (2)$$

Preparation of ESHANP

Ultrasonic irradiation was used to prepare ESHANP by neutralization method. In this respect, the calcium hydroxide suspension was allowed to expose to an ultrasonic irradiation source of 50 W (30 kHz, Cole-Parmer, Model 8893, Ultrasonic, Germany) at high frequencies for 2 h. While undergoing a second 2 h of ultrasonic irradiation; a suitable amount of 85 weight% Ortho-phosphoric acid was slowly added at a precise rate drop by drop to $Ca(OH)_2$ suspension under a high speed mechanical stirrer (Heidolph Instrument, Type RZR1, 280–2200 1/min, Germany). Until the H^+ ion concentration of the reaction solution was about neutrality under the continuous stirring. The molar ratio of Ca/P was 1.67:1, where the H_3PO_4 solution was added to the calcium precursor at a rate of 10–15 drops/min.

The solution was continual flipping for a 2nd time of 30 min, finally it aged for 24 h. This could assist to get a complete precipitation process as obtained by the next Eq. (3) [22]:

$$10Ca(OH)_2 + 6H_3PO_4 \rightarrow Ca_{10}(PO_4)_6(OH)_2 + 18H_2O \quad (3)$$

High speed mechanical stirrer with the slowly reagent addition facilitate pH control and avoiding a local inhomogeneity. The resulting slurry was discrete by centrifugation, then it was washed carefully by DDW. The resultant powder was filtered and dried in the oven for 24 h at 80 °C (denoted ESHANP-80**).** A part of the dried precipitate was calcined at 850 °C for 4 h (denoted CESHA-850). Finally, the white crystalline agglomerates were found in the crucible.

Characterization of material

The morphological characterization and the phase structure of the samples was studied by TEM (JEM-2100) and BET measurements (NOVA 1000e, USA). Spectroscopic analysis of the powders were determined using Fourier transformed infrared spectra FT-IR (Thermo, USA) of ESHANP-80 and CESHA-850 over a range of 400–4000 cm^{-1} with the KBr (potassium bromide) disk method. Thermal stability was processed using thermo gravimetric analysis-differential thermal analysis TG-DTA (SDTQ600, TA Instruments, New Castle, DE, USA) from room temperature to 1000 °C using a heating rate of 20 °C/min. The elemental constituent of the HA (% weight of each element) was conducted by energy dispersive X-ray spectroscopy (EDX, JEOL-JSM 5600LV, Japan). X-ray diffraction Shimadzu 6000, Japan, $Cu_{k\alpha}$ = 1.5Å radiation generated at a voltage of 40 kV and a current of 30 mA. Data were collected in the 2Θ range of 4°–90° at a scan speed of 8 deg. min^{-1}.

Sorption procedures

Individual sorption studies of ^{60}Co(II), Cd(II), ^{99}Mo and ^{99m}Tc onto the synthesized sorbents was performed by shaking, in tightly closed polyethylene bottles, a 0.05 g of the synthesized samples with 5 ml aqueous solutions at various pH and constant initial ion concentration, 100 mg L^{-1} Co(II) and Cd(II). The starting pH value was adjusted using 0.1 M HCl and/or 0.1 M NaOH solution. The mixture was shaken in a thermostatic shaker at 25 ± 1 °C. At predetermined time periods, shaking was stopped, supernatants was discrete by centrifugation and subjected to radiometric assay to estimate the activity of the studied radionuclides (^{60}Co, ^{99}Mo and ^{99m}Tc). The concentration of Cd(II) ions was measured by atomic absorption spectrophotometer (AAS—M5 Model, from Thermo, UK). To verify the solubility extent of each ion (^{60}Co(II) and Cd(II)), additional pack of tests was performed. In these experimental sets, 5 ml of ion solutions of 100 mg L^{-1} of ^{60}Co(II) and Cd(II), was put individually in 25 ml glass bottles without adsorbent materials. Each set was dependent to the identical procedure and conditions of pH study. After equilibrium, the potential loss in radioactivity of metal ions from liquor with changing pH values was determined and attributed only to the precipitation of metal ions. These sets were denoted as "Blank study". An additional batch of experiments was conducted as a cursor of shaking time & primary ion concentration of ^{60}Co(II), Cd(II). The experimental results, throughout this work, were mathematically treated to calculate the uptake percent (U%) and the capacity (q, mg/g) using the following Eqs. (4, 5):

$$U\% = \frac{A_i - A_f}{A_i} \times 100 \tag{4}$$

$$q = \frac{U(\%)}{100} \times C_o \times \frac{V}{m} \tag{5}$$

where A_i and A_f are the initial and final radioactivity(or concentration in case of Cd) of the studied isotopes. The C_o is the initial concentration (mg/L) of metal ions, V is the volume of solution and m is the weight of the prepared nanomaterial.

All experimental data were the average of three individuals of each experiment and the reproducibility of experimental measurements were mostly within ± 3.8%.

Results and discussion

Characterization of ESHANP

The structural constituents (weight%) of the chemically produced hydroxyapatite powder (ESHANP-80 and CESHA-850) are determined by EDX as indicated in Fig. 1. The EDX result shows the weight percentage of 46.0, 19.99 and 34.01% for O, P and Ca, respectively, in the ESHANP sample. The CESHA has consisted of 39.74, 22.37 and 37.89% for O, P and Ca, respectively. The ratio of Ca/P ranged from 1.69 to 1.70 for ESHANP-80 and CESHA-850 respectively, convenient with the reported values for hydroxyapatite powder [$Ca_5(PO_4)_3(OH)$]. The ideal Ca/P ratio of hydroxyapatite is 1.67 [23]. The hydroxyapatite Ca/P ratio derived from eggshells is generally assumed to be ≥1.67 [24]. XRD pattern (as seen in Fig. 1) indicates exist of fingerprint hydroxyapatite material that is coincident with those reported by [25, 26] and the morphology of the prepared hydroxyapatite is crystalline form. The crystallite size (D) of the ESHANP-80 nanoparticles was calculated using Scherrer's formula;

$$D = \frac{K\lambda}{\beta \cos\theta} \tag{6}$$

where k is the Scherrer constant (0.9), λ is the X-ray wave length (CuKα-1.54 Å) and β is the angular width of the diffracted peak with full width at half maximum (FWHM) in radians for the diffraction angle (2θ). The average crystallite

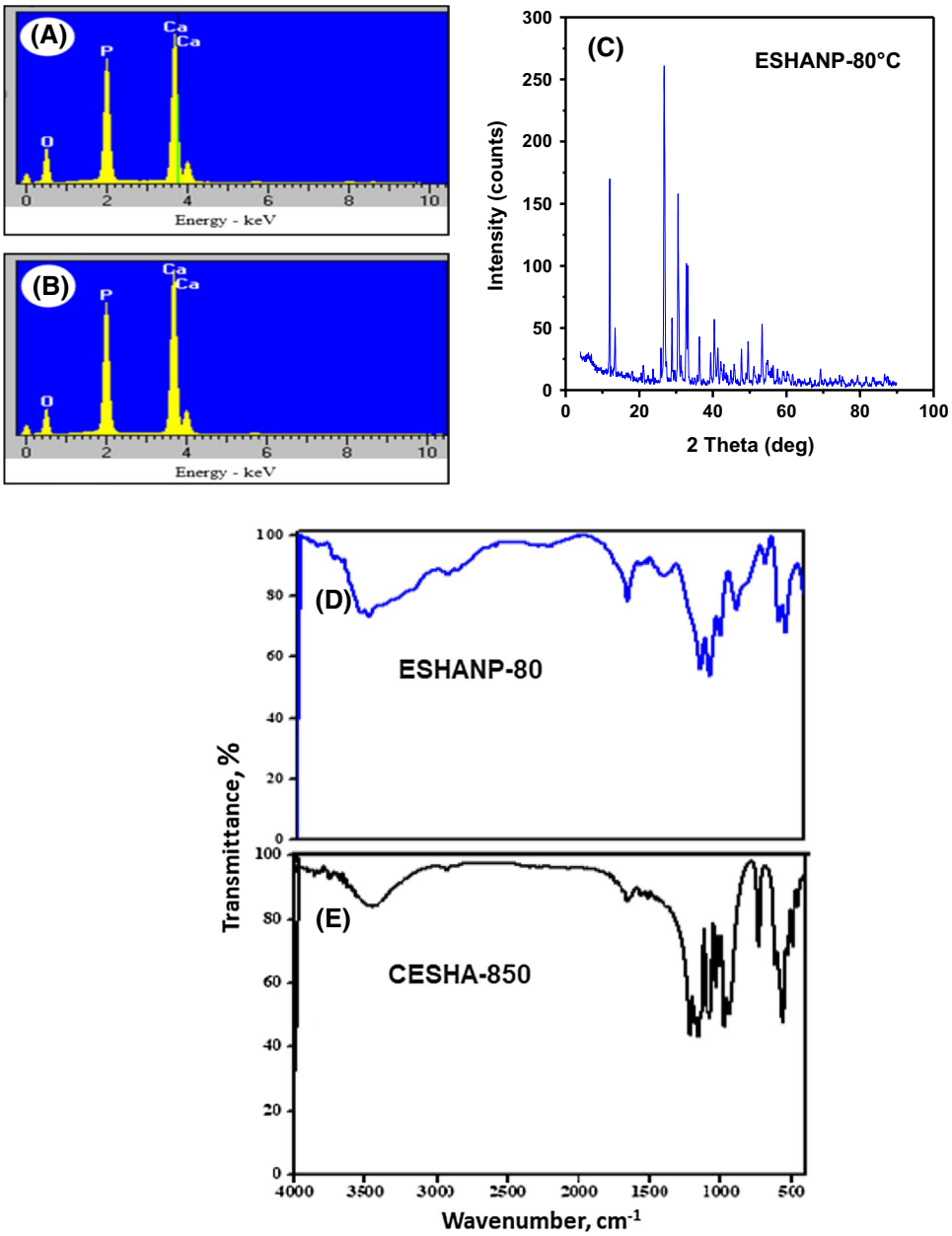

Fig. 1 Characterization of prepared materials by EDX analysis (**a** ESHANP-80, **b** CESHA-850), **c** XRD of ESHANP-80 and FTIR spectra of hydroxyapatite **d** ESHANP-80 and **e** CESHA-850

sizes determined from most intense peaks at 26.79 degrees (2θ). Calculated crystallite size is ~22.23 nm. It is confirmed prepared nanoparticles of ESHANP-80. The calcined hydroxyapatite (CESHA-850) has similar characteristic peaks with ESHANP-80 nano particle.

The infrared spectral analysis of the synthesized hydroxyapatite powders before (ESHANP-80) and after calcination (CESHA-850) were obtained in Fig. 1. ESHANP-80 exhibits characteristic stretching and vibrational modes of OH^- groups at 3541.89 cm^{-1} and 670.36 cm^{-1}. These absorption bands, which are also known as OH^- characteristic peak of hydroxyapatite [27], declare as aspect as they overlapped with water absorption bands. whereas other peaks of hydroxyapatite exist in the internal modes of asymmetrical stretching vibration corresponding to the PO_4^{3-} groups occur at: 1131.03 and 1065.86 cm^{-1}, 990.02 $cm^{-1,}$ 575.81 and 526.16 cm^{-1} and 469 cm^{-1} corresponding to that of ESHANP [28, 29]. The bands at 1131 and 1065 cm^{-1} can be attributed to the antisymmetric stretching of the P–O band. The 990 cm^{-1} band can be characterized the symmetric stretching of the P–O band. The bands at 575 cm^{-1} and 526 cm^{-1} are accompanied with the vibration of O–P–O bond, and the bands at 469 cm^{-1} may be related with the bending of O–P–O bond [30]. A wide absorption band was observed with an explicit peak at 3485.56 and 1649.51 cm^{-1} correspond to adsorbed H_2O [29, 31]. While bands at 876.33, 1511.39 and 1388.66 cm^{-1} are that of CO_3^{2-} ions which suggest incorporation of CO_3^{2-} ion

in synthesized hydroxyapatite [30, 32, 33]. According to [34]; C-O is stretching vibration for carbonate group usually appeared at wavenumber 1400–1600 cm^{-1}. However, the most significant stretching peak at 3541 cm^{-1}, followed by ESHANP-80 sample. Hydroxyapatite has strongly indicated exist of the OH^- stretching band in the samples.

The corresponding infrared spectra of thermal treated samples after heating at 850 °C in a furnace are clarified in Fig. 1e. Compared to the spectrum of the samples before heat treatment, in Fig. 1d, e, since several absorption peaks had disappeared. The most significant absorption bands to disappear were CO_3^{2-} adsorption bands which were previously most distinguished at 876 and 1388 cm^{-1} and water absorption bands at 3485 & 1649 cm^{-1} in Fig. 1d. These peaks are ill defined which confirms the elimination of CO_3^{2-} and H_2O because of the calcination of hydroxyapatite at temperature of 850 °C. The heat treatment had evidently removed the water molecules. All characteristic operative groups of hydroxyapatite, namely OH^- and PO_4^{3-} groups, were observed explicitly. In addition, substitution groups as CO_3^{2-} had disappeared due to heat treatment. This highly evidence that the heat treatment of powders made at 850 °C results in stoichiometric ESHANP. The higher intensity of hydroxyapatite characteristic peaks in samples ESHANP-80 and CESHA-850 proves that the higher rotational speed forms chemically more complete hydroxyapatite groups.

The morphologies of the co-precipitated produced powders (ESHANP-80) and heat treated (CESHA-850) observed by TEM, are seen in Fig. 2a, b. The range of nanosized diameter of (14.47–22.28 nm) and (12.17–39.11 nm) for ESHANP-80 and CESHA-850, respectively. It indicates that the prepared hydroxyapatite samples consisting of the particles with homogeneous and fine grain of components. The aggregates granular apatite (CESHA-850) is composed of different shapes as short, long columns, thick like plates and has flaked like morphology of relatively larger size [35]. The BET-surface area of the prepared material (ESHANP-80) was measured by N_2 adsorption/desorption isotherms experiment. It was found that the SH1 has a specific area reached 11.84 $m^2\ g^{-1}$ and average pore size of 41.71 nm. It can be confirmed preparation of nanoparticles from eggshell as biomass waste according to calculated crystalline size

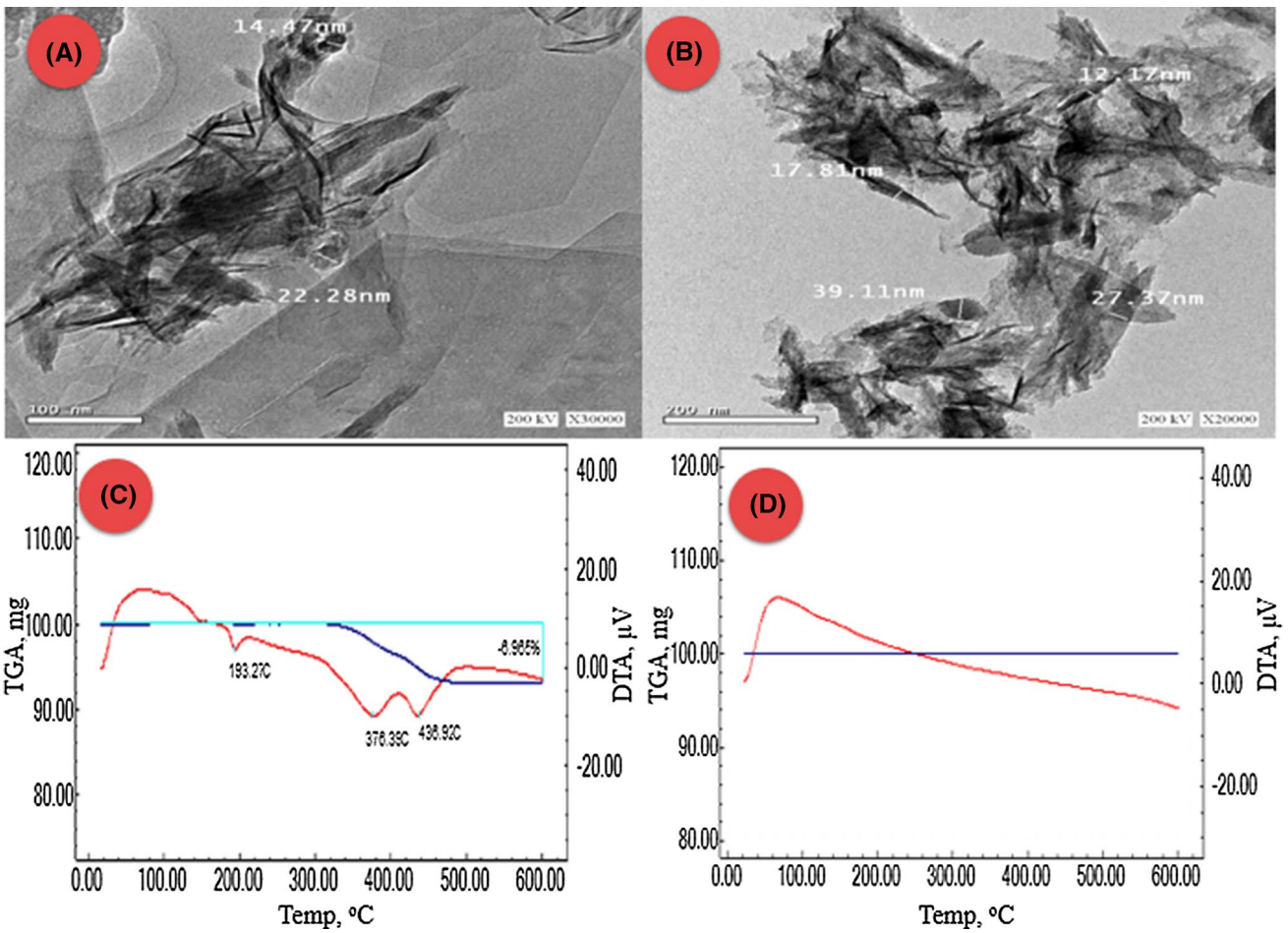

Fig. 2 The TEM images of ESHANP-80 (**a**), ESHANP-850 (**b**), TG-DTA curves of (**c**) ESHANP-80 (**c**) and CESHA-850 (**d**) samples

Scherrer's formula (XRD analysis), TEM and BET surface analysis. Thermal analysis DTA-TG was used to investigate the thermal properties of the hydroxyapatite samples. It can be clearly observed from the DTA-TG analysis (Fig. 2c, d), that there is a weight loss of about 6.96% up to 600 °C, which is consequent to the physical absorption of water. The DTA of the ESHANP-80 sample has shown three peaks at 193.27 °C attributed to interstalial water, 376.39 °C and 436.92 °C might be decomposition of ESHANP-80 material and transformation to $Ca_3(PO_4)_2$ and CaO (CESHA material). The thermal analysis of CESHA-850 material demonstrated that confirm a thermal stability of this material as shown in Fig. 2d. More or less stable curvature was observed including the temperature range, which shows the thermal steadiness of hydroxyapatite powder.

Sorption behavior

Effect of pH

The pH values of the solution are identified as an effective important parameter that led to changes the species of ions and the charged of the exterior of adsorbent. It is influencing the adsorption of metals on different sorbents. The uptake% of some radionuclides such as (^{60}Co, Cd(II), ^{99}Mo and ^{99m}Tc) onto CESHA and ESHANP at various initial pH values of the solution was studied as shown in Fig. 3. It was seen similar sorption behavior for Co(II) and Cd(II) onto CESHA and ESHANP adsorbents. The both prepared adsorbent of CESHA and ESHANP have no affinity to adsorb ^{99}Mo and ^{99m}Tc. The Fig. 3 also clarify that high sorption characteristic for ESHANP than CESHA towards Co(II) and Cd(II) ions. Uptake% of them is increased by increasing pH at the range of 1-3. It is noticed that a little rise in the uptake% by continuous increase the pH (3–8) of solution. The speciation of Co, Cd, Mo and Tc in aqueous solution is illustrated in S1. The predominant cationic species of Co^{2+}, Cd^{2+} and anionic species of $HMoO_4^-$, MoO_4^{2-} and TcO_4^- exist in this experimental condition. It is expected that the sorption of ^{99}Mo and ^{99m}Tc might be limited to the electrostatic attraction between their anionic species and the positive charged sites on the surface of nanoparticles of hydroxyapatite. These evidences argue that the electrostatic attraction between Co(II) and Cd(II) ions and the positively charged site of sample surface was unfavorable interaction over the initial pH range1–9. The sorption of ^{60}Co(II) or Cd(II) on CESHA is decreased the final pH values as shown in Fig. 3e, f. It is indicated that sorption of ^{60}Co(II) and Cd(II) resulted in a proton liberation from the surface active sites of the applied sample in the aqueous solution. The difference in sorption behavior of Co and Mo is attributed to their ionic radius which means the smaller ionic radius of ^{60}Co is easier and faster than ^{99}Mo on the sorption site of the prepared nanomaterials. In addition, the ESHANP adsorbent exhibit higher sorption affinity towards ^{60}Co than Cd(II) at optimum pH 4.5. It was noticed that the ^{60}Co(II) in the blank sample has been started precipitate at pH > 6 as demonstrated in Fig. 3a. Hence, it was adjusted the pH values of aqueous solution in more sorption attempts at pH 4.5.

Effect of shaking time

The shaking time is one of the major efficient factors in the adsorption process of ions. Thus, the sorption kinetics of Co and Cd from aqueous solution of pH 4.5 at the 25 ± 1 °C onto the prepared CESHA and ESHANP was studied as obtained in Fig. 4a, b. Uptake% is gradually raised by rising the time till 1 h, then a slow increased of uptake% from 1 h till 24 h. After that, it is noticed by increase the shaking time didn't effect on the uptake%. The consequences are demonstrated various sorption performances of radionuclides using CESHA and ESHANP as adsorbent materials. The potential sorption of ESHANP is higher than CESHA towards the radionuclides under study. It is attributed to water content of ESHANP that might be played a significant role in the sorption of Co and Cd. The maximum uptake of Cd is 87.7% and 13.7% onto ESHANP and CESHA, respectively. While the maximum sorption of Co is 93.1% and 10.4% using ESHANP and CESHA, respectively. The 24 h is chosen as the equilibrium time for more sorption attempts.

Sorption kinetics

Rate interaction

The sorption kinetics process of ^{60}Co and Cd onto the prepared ESHANP and CESHA materials were studied. The sorption kinetics normally includes two stages: a rapid removal stage followed by much slower one before the equilibrium is attained. Assuming pseudo-first-order kinetics, the rate of the sorptive interactions can be evaluated by the simple Lagergren Eq. (7) [36]:

$$\log(q_e - q_t) = \log q_e - \frac{k_f}{2.303} t \quad (7)$$

where q_e and q_t are the amount of ^{60}Co(II) and Cd(II) adsorbed on the synthesized sorbents at equilibrium & time t (mg g^{-1}), and k_f is the pseudo-first-order rate constant (min^{-1}). The plot of log (q_e−q_t) versus t for removal of ^{60}Co(II) and Cd(II) onto ESHANP and CESHA materials is obvious in Fig. 4c, d. The values of (k_f) and q_e were evaluated from the slope and intercept, respectively, of the obtained straight lines as reported in Table 1. The data showed the calculated q_e values of the ^{60}Co(II) and Cd(II) adsorbed using the pseudo-first-order kinetic model, were

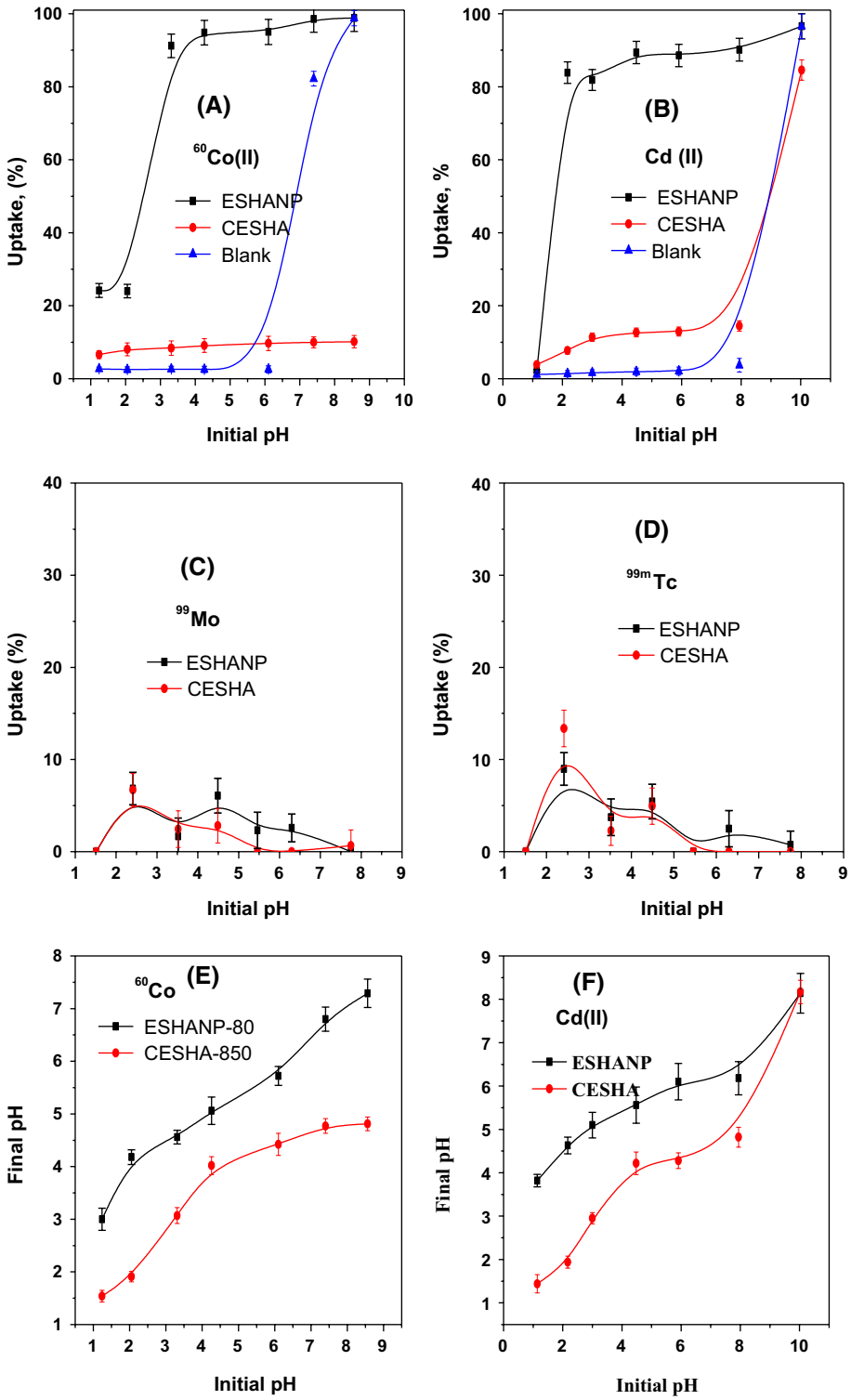

Fig. 3 Effect of initial pH on uptake percent of ^{60}Co(II), Cd(II), ^{99}Mo and ^{99m}Tc on the prepared ESHANP and CESHA materials at (C_o=100 ppm, t_{eq}= 24 h, V/m = 100 mLg^{-1}, temp = 25±1 °C)

not consisted with the experimental q_e values. This confirms that the removal of ^{60}Co(II) and Cd(II) using the ESHANP and CESHA materials did not follow the pseudo-first-order model although the high correlation coefficients (R^2). Therefore, a pseudo-second-order kinetic model was applied. The linear pseudo-second-order kinetics was represented by the following [37]:

$$\frac{t}{q_t} = \frac{1}{k_s q_e^2} + \frac{1}{q_e} t \quad (8)$$

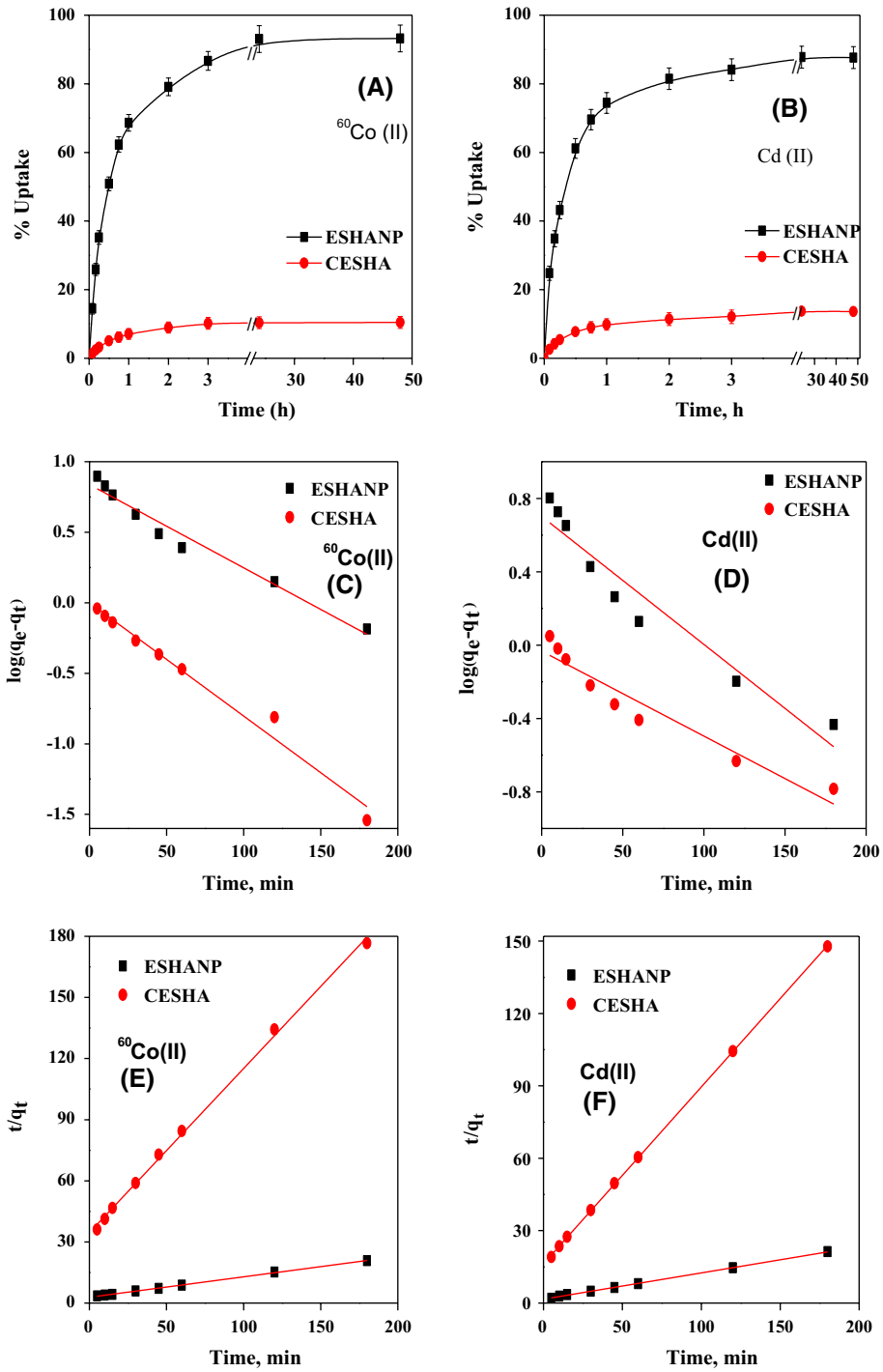

Fig. 4 Kinetic profile: **a**, **b** Effect of contact time on uptake percent of ^{60}Co and Cd, **c**, **d** Lagergren plots for sorption of ^{60}Co and Cd, **e**, **f** Pseudo–second– order plots for sorption of ^{60}Co and Cd on the prepared ESHANP and CESHA materials at (C_o=100 ppm, V/m = 100 mLg^{-1}, temp= 25±1 °C, pH = 4.5)

where k_s is the rate constant of pseudo-second-order (g mg^{-1} min^{-1}). If the initial sorption rate (h, mg g^{-1} min^{-1}) equals $k_s q_e^2$, then Eq. (8) becomes:

$$\frac{t}{q_t} = \frac{1}{h} + \frac{1}{q_e} t \tag{9}$$

Plotting of t/q_t versus t for the removal of ^{60}Co(II) and Cd(II) on ESHANP and CESHA materials gave a linear relevance as shown in Fig. 4e, f. The values of the pseudo-second-order model parameters were computed from the intercept and the slope of the straight lines of the analogous plots. The obtained data was illustrated that R^2 value is excessively high and closest to 1 (R^2 = 0.999) for the pseudo-second-order kinetic model compared with that for the pseudo-first-order kinetic model. The modeled q_e values for removal of ^{60}Co(II) and Cd(II) ions on ESHANP and CESHA materials

Table 1 Kinetics parameters for sorption of ^{60}Co(II) and Cd(II) ions by different prepared adsorbents

Elements	Kinetic parameters		Sample	
^{60}Co(II)	Model	Parameters	ESHANP	CESHA
	Experimental	qe (mg g^{-1})	9.32	1.05
	Pseudo-First order	K_f ($mg^{(1-1/n)}$ $L^{1/n}$ g^{-1})	0.014	0.019
		q_e (mg g^{-1})	6.88	1.00
		R^2	0.965	0.977
		S.D.	0.0004	0.0004
	Pseudo-second order	k_s (g mg^{-1} min^{-1})	0.003	0.018
		h (mg g^{-1} min^{-1})	0.35	0.03
		q_e (mg g^{-1})	9.97	1.24
		R^2	0.999	0.998
		S.D.	0.0009	0.01
	Elovich	α (g mg^{-1} min^{-2})	0.18	1.09
		β (mg g^{-1} min^{-1})	2.09	0.25
		R^2	0.993	0.988
		S.D	0.16	0. 02
Cd(II)	Experimental	qe (mg g^{-1})	8.83	1.38
	Pseudo-First order	K_f ($mg^{(1-1/n)}$ $L^{1/n}$ g^{-1})	0.16	0.11
		q_e (mg g^{-1})	5.03	0.93
		R^2	0.922	0.919
		S.D.	0.0007	0.0005
	Pseudo-second order	k_s (g mg^{-1} min^{-1})	0.007	0.033
		h (mg g^{-1} min^{-1})	0.62	0.06
		q_e (mg g^{-1})	9.19	1.36
		R^2	0.999	0.999
		S.D.	0.0009	0.003
	Elovich	α (g mg^{-1} min^{-2})	0.47	1.18
		β (mg g^{-1} min^{-1})	1.8	0.28
		R^2	0.967	0.992
		S.D	0.29	0.02

at equilibrium were compatible with the experimental results, Table 1. Thus, it deduced that the sorption kinetics could be delineated by the pseudo-second-order model. So, the rate determining step in the sorption of ^{60}Co(II) and Cd(II) on ESHANP and CESHA materials is a chemisorption process depends on both initial concentrations of metal ions and a number of effective positions in sorbent surface.

Elovich equation is often employed to clarify the adsorption kinetics and successfully demonstrate the chemisorption on heterogeneous sorbents. The linear Eq. (10) is reported by [38]:

$$q_t = 2.303\beta log(\alpha\beta) + 2.303\beta log t \quad (10)$$

where α and β are Elovich coefficients show the initial sorption rate (g mg^{-1} min^{-2}) and the desorption constant (mg g^{-1} min^{-1}), respectively.

The relation between q_t and log t for removal of ^{60}Co and Cd onto the prepared ESHANP and CESHA adsorbent materials is demonstrated in Fig. 5a, b. The plots exhibit good linear relations from their slops and intercepts Elovich constants were determined and given Table 1. These values represent the rate of chemisorption of sorption α and constant β is regarding to the exterior covered [39]. Although Elovich equation is useful in describing the chemical sorption on heterogeneous systems, no definite mechanism for ^{60}Co and Cd(II) adsorbent interaction could be suggested. Thus, it is predicted that ^{60}Co and Cd(II) is held strongly to the composite surface by chemisorptive bonds.

Mass transport kinetics

Intra-particle diffusion The solute transport from the solution phase of the exterior of sorbent particles occurs in several steps. The sorption method may be ruled either by one or more steps, e.g. pore diffusion or envelope diffusion and adsorption on the pore surface, or a summation of more than one step. Generally, the sorption process could be considered as diffusion controlled if its rate is entrusted upon the rate at which analyte diffuse towards the adsorbent surface.

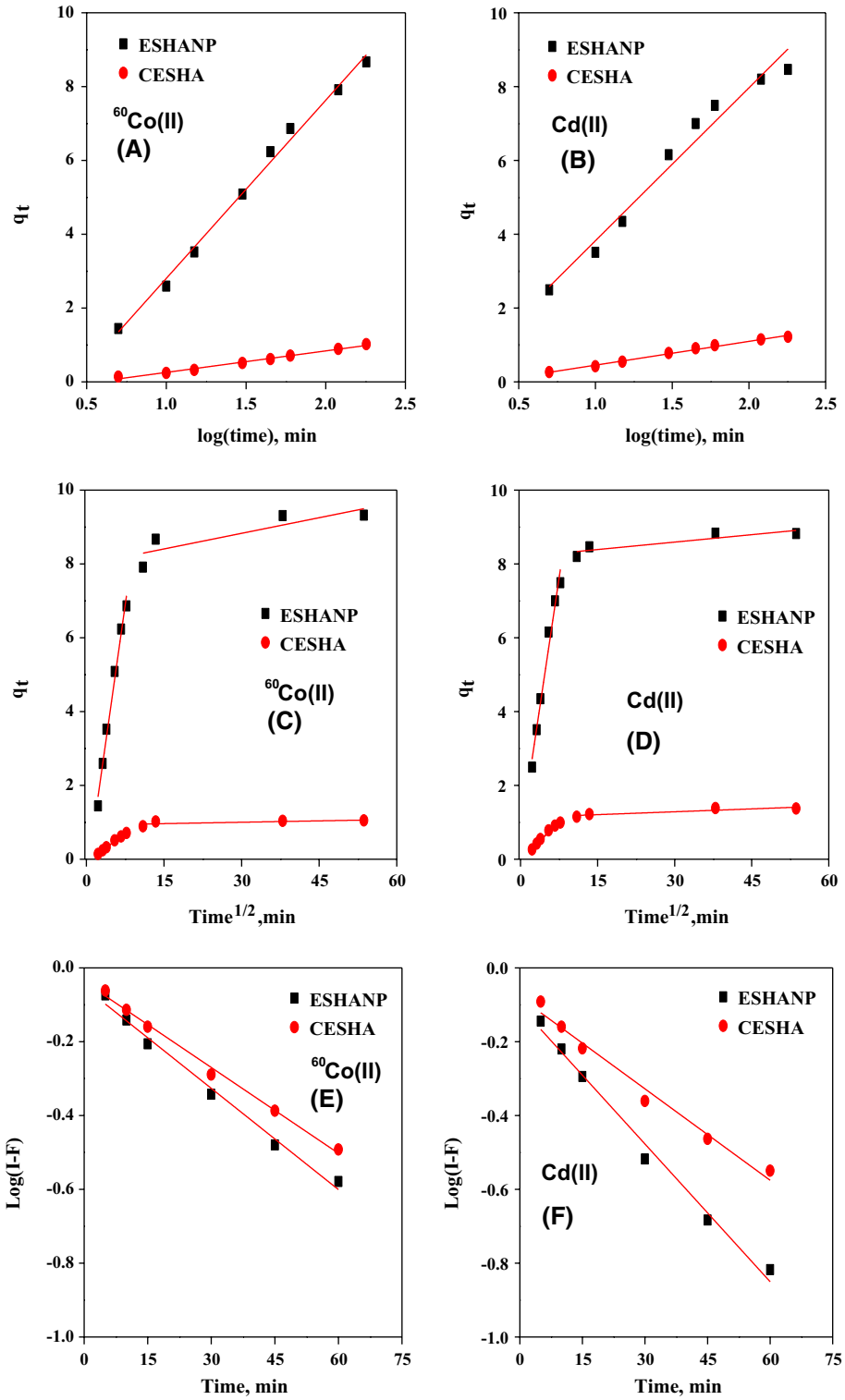

Fig. 5 **a**, **b** Elovich plots, **c**, **d** Weber-Morris plots and **e**, **f** Boyed plots for sorption of ^{60}Co and Cd onto the synthesized ESHANP and CESHA materials sorbents (eq. time = 24 h, V/m = 100 mL.g^{-1}, temp = 25±1 °C, pH = 4.5)

The probability of intra-particle diffusion was tested by [40] using the following Eq. (11):

$$q_t = k_{id} t^{0.5} + C \tag{11}$$

where k_{id} is the intra-particle diffusion rate constant (mg g^{-1} min$^{-0.5}$). C is a constant (mg g^{-1}) gives a concept about the thickness of the border layer, i.e., larger the value of C the greater is the border layer effect.

If the Weber–Morris plot of q_t versus $t^{0.5}$ gives a straight line pass through origin, then the sorption process is governed by intra-particle diffusion only. However, if the results display multi-linear plots, then it deduced that more than one

step controlled in the sorption process. The intra-particle diffusion plots of ^{60}Co(II) and Cd(II) sorbed per unit mass of sorbent versus $t^{0.5}$ are shown in Fig. 5c, d. The slopes of these plots are known as a rate characteristic parameter of the adsorption when the rate controlling is the intra-particle diffusion. The graphs reveal data points related by two straight lines, the first portion depicting macropore diffusion and the second representing micro-pore diffusion. The thickness of boundary layer was measured from the intercepts that given to the y-axis. The aberration of straight lines from the origin is attributed to various amounts of mass transfer from the initial to the final steps of sorption. It is also established that the pore diffusion is not only the rate-predominant step. The sorption data for q_e versus $t^{1/2}$ for the inceptive period show curvature, usually related to border layer diffusion effects or external mass transfer effects. The values of rate parameters (k_{id1} and k_{id2}) were evaluated from the slopes of the linear plots and registered in Table 2. The rate constant of intra-particle diffusion for the first linear segment (k_{id1}) had the higher values than the second linear segment k_{id2} for ^{60}Co(II) and Cd(II) onto both prepared adsorbents. It is proposed that a number of for ^{60}Co(II) and Cd(II) spread into the pores before being sorbed. It can conclude that intra-particle diffusion may not be the predominant agent in assessment the kinetics of the process.

Liquid particle diffusion When the transport of solute molecules from a liquid phase to a solid phase boundary plays a significant role in the sorption process, the liquid film diffusion model may be utilized using the Eq. (12) reported by [41]:

$$\log(1-F) = \frac{k_{fd}}{2.303}t \tag{12}$$

where F is the partial achieving of balance ($F = q_t / q_e$). k_{fd} is the film diffusion rate constant.

A linear plot of log (1−F) versus t with zero intercept could propose that the kinetics of the sorption process are governed by diffusion within the liquid film contour the solid sorbent. The plots of log (1−F) versus t are shown in Fig. 5e, f. The curves exhibit linear plots. The rate constant for liquid film diffusion, k_{fd}, was computed from the slope of the linear relations and recorded in Table 2. The rate constant for liquid film diffusion, k_{fd}, is in the range of 0.018–0.02 min^{-1}, 0.019–0.029 min^{-1} for ^{60}Co(II) and Cd(II), respectively. From these data, the lower values of rate constant are rated constant of film diffusion. The non-zero intercepts show again that despite giving linear plots, the predictions of the model will have only limited applicability in sorption of for ^{60}Co(II) and Cd(II) on the prepared ESHANP and CESHA adsorbent materials.

Sorption isotherm

Sorption isotherms are empirical models describing the relation between equilibrium concentration of the adsorbate and the amount adsorbed on the solid surface at constant temperature. The sorption isotherms for Cd and Co removal were studied using initial concentrations of ^{60}Co and ^{109}Cd ranging from 100-500 mg L^{-1} as giving in Fig. 6a, b. The results are revealed that the maximum capacity (q_e) of 16.91 mg g^{-1} and 13.84 mgg^{-1} for ^{60}Co and Cd, respectively, using the ESHANP-80 adsorbent material. The low sorption capacity affinity of CESHA-850 adsorbent material is 2.48 mg g^{-1} and 3.39 mg g^{-1} for ^{60}Co and Cd, respectively, has confirmed the previous obtained results. The ESHANP-80 that was prepared according to Eq. (3) and have the chemical formula of $Ca_{10}(PO4)_6$ $(OH)_2$. The hydroxyl group (OH^-) has played a significant role for the sorption characteristic of ESHANP-80

Table 2 Different diffusion rate constants for sorption of ^{60}Co(II) and Cd(II) ions onto the prepared adsorbents

		Co(II)				Cd(II)			
		ESHANP		CESHA		ESHANP		CESHA	
		1*	2**	1*	2**	1*	2**	1*	2**
Intra-particle diffusion	k_{id} (mgg^{-1} min$^{0.5}$)	0.99	0.03	0.1	0.002	0.93	0.01	0.008	0.002
	Intercept	−0.52	7.98	−0.087	0.93	0.62	8.19	0.004	1.13
	R^2	0.987	0.624	0.996	0.262	0.976	0.711	0.981	0.775
	SD	0.05	0.01	0.003	0.002	0.06	0.004	0.13	0.005
Film diffusion	k_{fd} (min^{-1})	0.02		0.018		0.029		0.019	
	Intercept	−0.10		−0.08		−0.10		−0.08	
	R^2	0.989		0.994		0.987		0.977	
	SD	0.0005		0.0003		0.0006		0.0005	

*First linear segment

**Second linear segment

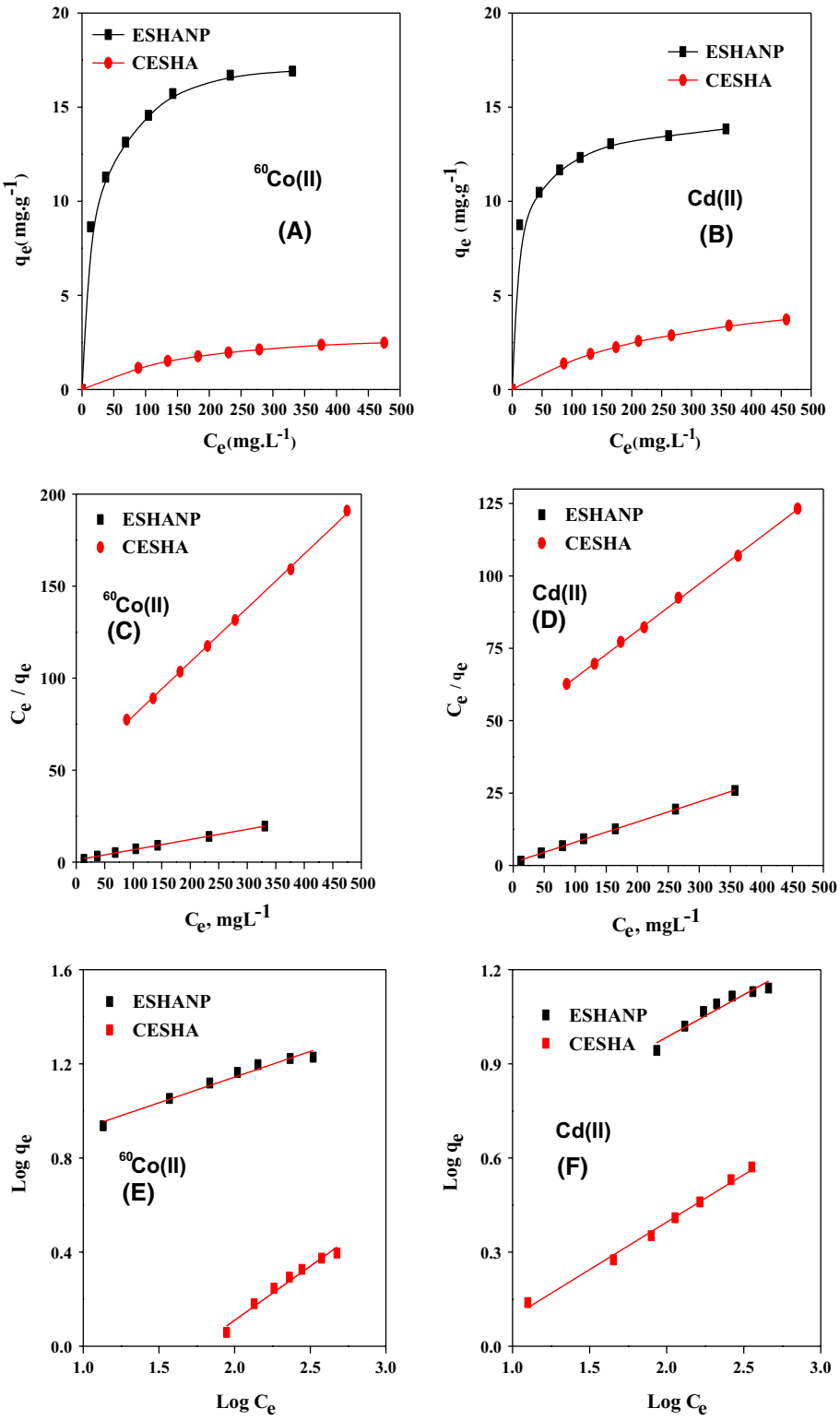

Fig. 6 **a**, **b** Adsorption isotherm for ^{60}Co(II) and Cd(II) ions, **c**, **d** Langmuir plot and **e**, **f** Freundlich plot for sorption of ^{60}Co and Cd onto the prepared ESHANP and CESHA materials sorbents (eq. time = 24 h, V/m = 100 mL.g^{-1}, temp = 25±1 °C, pH = 4.5)

nanoparticles rather than the CESHA-850 nanoparticles. Whereas, the CESHA-850 was lost the OH during the calcination process that led to the formation of $Ca_3(PO_4)_2$ and CaO according to suggested reaction:

$$Ca_{10}(PO_4)_6(OH)_2 \underline{\Delta} 3Ca_3(PO_4)_2 + CaO + H_2O \quad (13)$$

This difference between both nanomaterials of hydroxyapatite might be explained the higher sorption capacity of ESHANP-80 than CESHA-850 nanoparticles towards the radionuclides or heavy metals under this study. Two isotherm of Freundlich and Langmuir isotherm models were selected to anatomize the experimental findings in this investigation.

Langmuir model

The Langmuir isotherm model is established in the imposing of monolayer coverage of adsorbate ions onto the adsorbent surface. The mathematical linear form of this model is [42, 43]:

$$\frac{C_e}{q_e} = \frac{1}{k_L Q_{\max}} + \frac{C_e}{Q_{\max}} \tag{14}$$

where $Q_{\max}$ is the maximum adsorbed amount of of ^{60}Co and ^{109}Cd onto ESHANP and CESHA adsorbent materials (mg g^{-1}) and k_L is Langmuir constant that is concerning to the sorption strength (L mg^{-1}). The relation between $\frac{C_e}{q_e}$ and C_e for sorption of ^{60}Co(II) and Cd(II) onto the ESHANP and CESHA adsorbent materials is seen in Fig. 6c, d. The amount of Langmuir isotherm model's constants is accounted from the slopes and intercepts of the straight lines of the analogous plots and their values along with the correlation coefficients (R^2) are reported in Table 3. It is explicit that the values of R^2 are high and closest to 1 ($R^2 = 0.999$). The calculated maximum sorption capacity ($Q_{\max}$)of ESHANP and CESHA adsorbents materials using the Langmuir isotherm model are agreeable with the experimental $Q_{\max}$ values for sorption of ^{60}Co(II) and Cd(II). Based on these results, the sorption isotherm of ^{60}Co(II) and Cd(II) onto the ESHANP and CESHA adsorbent materials can be explained more favorably by Langmuir isotherm model. Therefore, a chemisorption process is expected to be occurred between ^{60}Co(II) and Cd(II) and sorbent surface. Also, a monolayer of ^{60}Co(II) and Cd(II) ions could be predicted to cover the surface of the ESHANP and CESHA adsorbent materials as well as the energy of sorption could be the same at all sites. The adsorbed metal ions were postulated to be affixed to a particular site on the solid surface and isn't free to move over the surface from one surface site to another.

Freundlich model

Freundlich isotherm model is applicable for excessively dissimilar surfaces anyway, it is adequate for sorption along a limited range of concentrations. Its linear equation is expressed as [44–46]:

$$\log q_e = \log k_f + \frac{1}{n} \log C_e \tag{15}$$

where C_e is the equilibrium concentration of ^{60}Co(II) and Cd(II) in solution (mg L^{-1}), k_f is the Freundlich isotherm constant ($mg^{(1-1/n)}$ $L^{1/n}$ g^{-1}) that is indicative of the relative sorption capacity and (1/n) is a Freundlich isotherm exponent constant towards the sorption intensity.

The relation between $\log q_e$ and $\log C_e$ for the sorption of ^{60}Co(II) and Cd(II) onto the ESHANP and CESHA adsorbent materials is displayed in Fig. 6e, f. The parameters amounts of the Freundlich isotherm were computed and the R^2 of their lines is recorded in Table 3. The obtained straight lines revealed that the sorption of ^{60}Co(II) and Cd(II) onto ESHANP and CESHA adsorbent materials may fit the investigated model. Freundlich isotherm parameter (1/n) that measures the sorption strength of ^{60}Co(II) and Cd(II) onto the applied sorbents showed values less than unity (0.599 and 0.547) indicating that the isotherms can be construed by a convex Freundlich isotherm [43, 46]. This denotes

Table 3 Langmuir and Freundlich isotherm constants for Co(II) and Cd(II) ions sorption onto the synthesized sorbents

Elements	Sample	Langmuir constants			R^2
		Q_{max} (mg g^{-1})	k_L (L mg^{-1})	SD	
Co(II)	ESHANP	17.99	0.048	0.0008	0.999
	CESHA	3.41	0.006	0.003	0.999
Cd(II)	ESHANP	14.31	0.067	0.0009	0.999
	CESHA	6.16	0.003	0.0015	0.999
Elements	Sample	Freundlich constants			R^2
		(k_F)	(*1/n*)	SD	
Co(II)	ESHANP	5.09	0.22	0.017	0.967
	CESHA	0.15	0.46	0.033	0.969
Cd(II)	ESHANP	2.77	0.27	0.033	0.917
	CESHA	0.62	0.30	0.010	0.993

Table 4 Comparison of sorption capacity for Co(II) and Cd(II) ions onto the synthesized sorbents

Elements	Sample	(q_e) (mg g^{-1})	Exp. conditions	References
Co(II)	SiO_2–Fe–CN nano-material	11.36	pH=5.5, V/M = 100, t = 1 h, T = 25 °C	[46]
	Mesoporous KZnFC	10.5	0.1 M HNO_3, V/M = 100, t = 1 h, T = 25 °C	[45]
	WTR	17.31	pH=6, V/M = 60, t = 48 h, T = 25 °C	[47]
	Area shell biomass	11.53	pH=2–7, V/M = 500, t = 2 h, T = 27 °C	[48]
	P(AM-AA-AN)-DAM/DtBB18C6	4.75	pH=5, V/M = 100, t = 2 h, T = 25 °C	[49]
	ESHANP	16.91	pH=4.5, V/M = 100, t = 24 h, T = 25 °C	This study
	CESHA	2.48		This study
Cd(II)	Fe_3O_4	9.40	pH=4.5, V/M = 200, t = 48 h, T = 25 °C	[50]
	NA-FeOx	5.98	pH=5.5, t = 8 h, T = 25 °C	[51]
	NA	12.4		
	RH	13.8	pH=8, V/M = 2000, t = 24 h, T = 20 °C	[52]
	MC	5.54		
	Modified goethite	11.91–15.83	pH=5.5, V/M = 400, t = 24 h, T = 25 °C	[53]
	Fiber	9.18	pH=4.2, V/M = 250, t = 24 h, T = 25 °C	[54]
	ESHANP	13.84	pH=4.5, V/M = 100, t = 24 h, T = 25 °C	This study
	CESHA	3.39		This study

that a meaningful sorption probably have a value even at high metal ion concentrations. The K_f values of ^{60}Co(II) and Cd(II) sorption onto ESHANP adsorbent materials are greater than that for sorption onto CESHA adsorbent materials. This confirms that ESHANP adsorbent materials have a greater sorption affinity towards ^{60}Co(II) and Cd(II) than CESHA adsorbent materials. Freundlich isotherm model has not predicted a saturation of the solid surface by ^{60}Co(II) and Cd(II) and so the exterior coverage being mathematically unlimited.

Comparison

The potential sorption capacity of ^{60}Co(II) and Cd(II) ions onto the prepared ESHANP and CESHA sorbents materials have been compared with others adsorbents materials as demonstrated in Table 4. The reported data in Table 4 is revealed that ESHANP and CESHA sorbents materials are efficient and economical adsorbent materials.

Conclusion

Nanoparticles of hydroxyapatite was successfully prepared from eggshell as a biomass waste. Potential sorption of some radioisotopes from aqueous solution onto ESHANP and CESHA prepared materials were evaluated. The results revealed that the ESHANP has higher sorption characteristic than CESHA materials towards Co and Cd from aqueous solution. The both prepared adsorbent of CESHA and ESHANP have no affinity to remove or adsorbed ^{99}Mo and ^{99m}Tc. The pseudo-second-order, intra-particle diffusion and Langmuir models were fitted and applicable to describe the sorption behavior of our studied. The prepared nanoparticles hydroxyapatite is promising and economic materials for wastewater treatment as well as for selective removal of activation products radioisotopes from nuclear waste sites. It is also demonstrate a promising materials for purification and separation of ^{60}Co from ^{99}Mo/^{99m}Tc.

Compliance with ethical standards

Conflicts of interest The authors declare that they have no compete of interest.

References

1. Dewiere L, Bugai D, Grenier C, Kashparov V, Ahamdach N (2004) Sr-90 migration to the geo-sphere from a waste burial in the Chernobyl exclusion zone. J Environ Radioact 74(1–3):139–150. https://doi.org/10.1016/j.jenvrad.2004.01.019
2. McKinley JP, Zachara JM, Smith SC, Liu C (2007) Cation exchange reactions controlling desorption of Sr-90 from coarse-grained contaminated sediments at the Hanford site, Washington. Geochim Cosmochim Acta 71(2):305–325. https://doi.org/10.1016/j.gca.2006.09.027
3. Zhang S, Niu H, Guo Z, Chen Z, Wang H, Xu J (2011) Impact of environmental conditions on the sorption behavior of radio cobalt in TiO_2/eggshell suspensions. J Radioanal Nucl Chem 289(2) 479–487. https://link.springer.com/article/10.1007/s10967-011-1088-9

4. Cecille L, Casarci M, Pietrelli L, New separation chemistry techniques for radioactive waste and other specific applications. Cambridge University Press, Cambridge (1991) https://www.springer.com/us/book/9789401136549
5. Elliott JC (1994) Structure and chemistry of the apatites and other calcium orthophosphates. Elsevier, Amsterdam
6. Oelkers EH, Montel JM (2008) Phosphates and nuclear waste storage. Elements 4(2):113–116. https://doi.org/10.2113/GSELEMENTS.4.2.113
7. Rakovan JF, Pasteris JDA (2015) Technological gem: materials, medical, and environmental mineralogy of apatite. Elements 11(3):195–200. https://doi.org/10.2113/gselements.11.3.195
8. Handley-Sidhu S, Renshaw JC, Moriyama S, Stolpe B, Mennan C, Bagheriasl S, Yong P, Stamboulis A, Paterson-Beedle M, Sasaki K, Pattrick RAD, Lead JR, Macaskie LE (2011) Uptake of Sr^{2+} and Co^{2+} into biogenic hydroxyapatite: implications for biomineral ion exchange synthesis. Environ Sci Technol 45(16):6985–6990. https://doi.org/10.1021/Es2015132
9. Moore RC, Sanchez C, Holt K, Zhao H, Xu HF, Choppinh GR (2004) Formation of hydroxyapatite in soil using calcium citrate and sodium phosphate for control of strontium migration. Radiochem Acta 92(9–11):719–723. https://doi.org/10.1524/ract.92.9.719.55000
10. Campayo L, Grandjean A, Coulon A, Delorme R, Vantelon D, Laurencin D (2011) Incorporation of iodates into hydroxyapatites a new approach for the confinement of radioactive iodine. J Mater Chem 21:17609–17911. http://pubs.rsc.org/en/content/articlelanding/2011/jm/c1jm14157k#!divAbstract
11. Coulon A, Laurencin D, Grandjean A, Coumes CCD, Rossognol S, Campayo L (2014) Immobilization of iodine into a hydroxyapatite structure prepared by cementation. J Mater Chem A 2:20923–20932. https://doi.org/10.1039/c4ta03236e
12. Wang DJ, Bradford SA, Paradelo M, Peijnenburg W, Zhou DM (2011) Facilitated transport of copper with hydroxyapatite nanoparticles in saturated sand. Soil Sci Soc Am J 76(2):375–388. https://doi.org/10.2136/sssaj.2011.0203
13. Thomson BM, Smith CL, Busch RD, Siegel MD, Baldwine C (2003) Removal of metals and radionuclides using apatite and other natural sorbents. J Environ Eng 129(6):492–499. https://doi.org/10.1061/(ASCE)0733-9372
14. Cui HB, Zhou J, Si YB, Mao JD, Zhao QG, Fang GD, Liang JN (2014) Immobilization of Cu and Cd in a contaminated soil: one- and four- year field effects. J Soil Sediments 14(8): 1397–1406. https://link.springer.com/article/10.1007%2Fs11368-014-0882-8
15. Li ZW, Zhou MM, Lin WD (2014) The research of nanoparticle and microparticle hydroxyapatite amendment in multiple heavy metals contaminated soil remediation. J Nano Mater. https://doi.org/10.1155/2014/168418
16. Smiciklas I (2010) Resource recovery of animal bones: study on sorptive properties and mechanism for Sr^{2+} ions. J Nucl Mater 400(1):15–24. https://doi.org/10.1016/j.jnucmat.2010.02.004
17. Meski S, Ziani S, Khireddine H, Meski S, Ziani S, Khireddine H (2010) Removal of lead ions by hydroxyapatite prepared from the egg shell. J Chem Eng Data 55(9): 3923–3928. https://pubs.acs.org/doi/abs/10.1021/je901070e
18. Wu HS, Tsou H, Hsu S, Liou S, Ho W (2013) A hydrothermal synthesis of eggshell and fruit waste extract to produce nanosized hydroxyapatite. Ceram Int 39(7):8183–8188. https://doi.org/10.1016/j.ceramint.2013.03.094
19. Rivera EM, Araiza M, Brostow W, Castaño VM, Díaz-Estrada J, Hernández R (1999) Synthesis of hydroxyapatite from eggshells. Mater Lett 41: 128–134. https://lapom.unt.edu/publications/pdf%20articles/varudadditions/MatLett_v41no3pp128-134.pdf
20. Ibrahim AR, Wei W, Zhang D, Wang H, Li J (2013) Conversion of waste eggshells to mesoporous hydroxyapatite nanoparticles with high surface area. Mater Lett 110:195–197. https://doi.org/10.1016/j.matlet.2013.08.014
21. Ahmed S, Ahsan M (2009) Synthesis of Ca-hydroxyapatite bioceramic from eggshell and its characterization. Bangladesh J Sci Ind Res 43:501–512. https://doi.org/10.3329/bjsir.v43i4.2240
22. Bahrololoom ME, Javidi M, Javadpour S, Ma J (2009) Characterization of natural hydroxyapatite extracted from bovine cortical bone ash. J Ceram Process Res 10:129–138
23. Benhayoune H, Charlier D, Jallot E, Laquerriere P, Balossier G, Bonhomme P (2001) Evaluation of the Ca/P concentration ratio in hydroxyapatite by STEM-EDXS: influence of the electron irradiation dose and temperature processing. J Phys D Appl Phys 34 141–147. http://iopscience.iop.org/article/10.1088/0022-3727/34/1/321/pdf
24. Akram M, Ahmed R, Shakir I, Ibrahim WAW, Hussain R (2014) Extracting hydroxyapatite and its precursors from natural resources. J Mater Sci 49(4):1461–1475. https://doi.org/10.1007/s10853-013-7864-x
25. Kamalanathan P, Ramesh S, Bang LT, Niakan A, Tan CY, Purbolaksono J, Chandran H, Teng WD (2014) Synthesis and sintering of hydroxyapatite derived from eggshells as a calcium precursor. Ceram Int 40:16349–16359. https://doi.org/10.1016/j.ceramint.2014.07.074
26. Charlena, Nuzulia NA, Handika (2017) Synthesis and characterization of composite hydroxyapatite-silver nanoparticles, IOP Conf. Series: Earth and Environmental Science 58: 012064. http://iopscience.iop.org/article/10.1088/1755-1315/58/1/012064/pdf
27. Berzina-Cimdina L, Borodajenko N, Research of calcium phosphates using Fourier transform infrared spectroscopy, Infrared Spectroscopy-Materials Science, Engineering and Technology, Rijeka, Croatia: InTech, (2012). 123–148. https://doi.org/10.5772/36942
28. Gergely G, Wéber F, Lukács I, Illés L, Tóth AL, Horváth ZE, Mihály J, Balázsi C (2010) Nanohydroxyapatite preparation from biogenic raw materials. Central Eur J Chem 8(2):375–381. https://doi.org/10.2478/s11532-010-0004-4
29. Ghosh SK, Prakash A, Datta S, Roy SK, Basu D (2010) Effect of fuel characteristics on synthesis of calcium hydroxyapatite by solution combustion route. Bull Mater Sci 33(1) 7–16. https://www.ias.ac.in/article/fulltext/boms/033/01/0007-0016
30. Koutsopoulos S (2002) Synthesis and characterization of hydroxyapatite crystals: a review study on the analytical methods. J Biomed Mater Res 62(4):600–612. https://doi.org/10.1002/jbm.10280
31. Ratner B, Hofman A, Schoen F (2004) Biomaterials science: an introduction to materials in medicine. Academic Press, New York
32. Shahmohammadi M, Jahandideh R, Behnamghader A, Rangie M (2010) Sol-gel synthesis of FHA/CDHA nanoparticles with a nonstochiometric ratio. Int J Nano Dim 1(1):41–45. https://doi.org/10.7508/IJND.2010.0X.004
33. Thamaraiselvi TV, Prabakaran K, Rajeswari S (2006) Synthesis of hydroxyapatite that mimic bone minerology. Trends Biomater Artif Organs 19(2):81–83
34. Meejoo S, Maneeprakorn W, Winotai P (2006) Phase and thermal stability of nanocrystalline hydroxyapatite prepared via microwave heating. Thermocim Acta 447(1):115–120. https://doi.org/10.1016/j.tca.2006.04.013
35. Poinescu AA, Ion RM, van Staden RI, van Staden JF, Ghiurea M (2010) Investigations on hydroxyapatite powder obtained by wet precipitation. SPIE Proceeding, Advanced Topics in Optoelectronics, Microelectronics and Nanotechnologies 7821:78210. https://doi.org/10.1117/12.882148
36. Lagergren S (1898) Zur theorie der sogenannten adsorption gelöster stoffe, Kungliga Svenska Vetenskapsakademiens, Handlingar, 24(4): 1–39

37. Ho YS, McKay G (1999) Pseudo-second order model for sorption processes. Process Biochem 34(5):451–465. https://doi.org/10.1016/S0032-9592(98)00112-5
38. Ho YS, McKay G (2002) Application of kinetic models to the sorption of copper(II) on to peat. Adsorp Sci Technol 20(8):797–815. https://doi.org/10.1260/026361702321104282
39. Teng H, Hsieh CT (1999) Activation energy for oxygen chemisorption on carbon at low temperatures. Ind Eng Chem Res 38(1):292–297. https://doi.org/10.1021/ie980107j
40. Weber WJ, Morris JC (1963) Kinetics of adsorption on carbon from solution. J Sanitary Eng Div Am Soc Civil Eng 89:31–60
41. Boyd GE, Adamson AW, Mayers LS (1947) The exchange adsorption of ions from aqueous solutions by organic zeolites. II. kinetics. J Am Chem Soc 69(11): 2836–2848. https://pubs.acs.org/doi/abs/10.1021/ja01203a066
42. Attallah MF, Allan KF, Mahmoud MR (2016) Synthesis of poly (Acrylic Acid-Maleic Acid)SiO_2/Al_2O_3 as novel composite material for cesium removal from acidic solutions. J Radioanal Nucl Chem 307: 1231–1241. https://link.springer.com/article/10.1007%2Fs10967-015-4349-1
43. Borai EH, Attallah MF, Elgazzar AH, El-Tabl AS (2018) Isotherm and kinetic sorption of some lanthanides and iron from aqueous solution by aluminum silicotitante exchanger. Part Sci Technol https://doi.org/10.1080/02726351.2017.1385550
44. El Afifi EM, Attallah MF, Borai EH (2016) Utilization of natural hematite as reactive barrier for immobilization of radionuclides from radioactive liquid waste. J Environ Radioact 151(1):156–165. https://doi.org/10.1016/j.jenvrad.2015.10.001
45. Rizk HE, Attallah MF, Ali AMI (2017) Investigations on sorption performance of some radionuclides, heavy metals and lanthanides using mesoporous adsorbent material. J Radioanal Nucl Chem 314:2475–2487. https://doi.org/10.1007/s10967-017-5620-4
46. Attallah MF, Abd-Elhamid AI, Ahmed IM, Aly HF (2018) Possible use of synthesized nano silica functionalized by Prussian blue as sorbent for removal of certain radionuclides from liquid radioactive waste. J Mol Liq 261:379–386. https://doi.org/10.1016/j.molliq.2018.04.050
47. Jiao J, Zhao J, Pei Y (2017) Adsorption of Co(II) from aqueous solutions by water treatment residuals. J Environ Sci 52:232–239. https://doi.org/10.1016/j.jes.2016.04.012
48. Parab H, Joshi S, Shenoy N, Lali A, Sarma US, Sudersanan M (2006) Determination of kinetic and equilibrium of Co(II), Cr(III), and Ni(II) onto coir pith. Process Biochem 41(3):609–615. https://doi.org/10.1016/j.procbio.2005.08.006
49. Shehata FA, Attallah MF, Borai EH, Hilal MA, Abo-Aly MM (2010) Sorption reaction mechanism of some hazardous radionuclides from mixed waste by impregnated crown ether onto polymeric resin. Appl Radiat Isot 68(2):239–249. https://doi.org/10.1016/j.apradiso.2009.10.040
50. Moussa SI (2013) Synthesis and characterization of novel magnetic nano-materials and studying their potential application in recovery of metal ions Ph.D. Thesis, Faculty of Science, Ain Shams Uni., Cairo, Egypt (2013). http://www.iaea.org/inis/collection/NCLCollectionStore/_Public/46/135/46135142.pdf
51. Silva-Yumia J, Escudey M, Gacitua M, Pizarro C (2018) Kinetics, adsorption and desorption of Cd(II) and Cu(II) on natural allophane: effect of iron oxide coating. Geoderma 319:70–79. https://doi.org/10.1016/j.geoderma.2017.12.038
52. Smolyakov BS, Sagidullin AK, Bychkov AL, Lomovsky IO, Lomovsky OI (2015) Humic-modified natural and synthetic carbon adsorbents for the removal of Cd(II) from aqueous solutions. J Environ Chem Eng V 3(3):1939–1946. https://doi.org/10.1016/j.jece.2015.07.005
53. Li W, Zhang S, Shan X (2007) Surface modification of goethite by phosphate for enhancement of Cu and Cd adsorption. Colloid Surf A Physicochem Eng Aspects 293(1–3):13–19. https://doi.org/10.1016/j.colsurfa.2006.07.002
54. Min SH, Han JS, Shin EW, Park JK (2004) Improvement of cadmium ion removal by base treatment of Juniper fiber. Water Res 38(5):1289–1295. https://doi.org/10.1016/j.watres.2003.11.016